Friction moment analysis of space gyroscope bearing with ribbon cage under ultra-low oscillatory motion

Jiang Shaona [a], Chen Xiaoyang [a,*], Gu Jiaming [b], Shen Xuejin [a]

[a] *Research Institute of Bearings, Shanghai University, Shanghai 200072, China*
[b] *Shanghai Tianan Bearing Co., Ltd, Shanghai 201108, China*

Abstract This paper presents the model of calculating the total friction moment of space gyroscope ball bearings which usually work under ultra-low oscillatory motion and are very sensitive to the friction moment. The aim is to know the proportion of the friction moment caused by each frictional source in the bearing's total friction moment, which is helpful to optimize the bearing design to deduce the friction moment. In the model, the cage dynamic equations considering six degree-of-freedom and the balls dynamic equations considering two degree-of-freedom were solved. The good trends with different loads between the measured friction moments and computational results prove that the model under constant rate was validated. The computational results show that when the speed was set at 5 r/min, the bearing's maximum total friction moment when oscillation occurred was obviously larger than that occurred at a constant rate. At the onset of each oscillatory motion, the proportion of the friction moment caused by cage in the bearing's total friction moment was very high, and it increased with the increasing speed. The analyses of different cage thicknesses and different clearances between cage pocket and ball show that smaller thickness and clearance were preferred.

1. Introduction

It is a continuous goal for bearing engineers to always develop advanced bearings that provide higher efficiency, lower friction, and more reliable, etc, under adverse operating conditions.[1] There is a considerable interest in understanding the friction moments of space gyroscope ball bearings used in many sensing mechanisms, such as those used for attitude control in spacecraft, which often run under ultra-low oscillatory motion for extended periods. Usually these bearings' starting

* Corresponding author. Tel.: +86 21 56331386.
 E-mail address: xychen@shu.edu.cn (X. Chen).
Peer review under responsibility of Editorial Committee of CJA.

friction moments are tested by particular friction moment tester[2] through frequent start-stop operation. From early papers,[3–10] as a result of frequent start-stop operation, the bearing's friction moment often traces out hysteresis loops which contain two regions, the pre-rolling and the steady rolling. Dahl[3,4] developed an empirical equation to describe the hysteresis behavior. Todd and Stevens,[5] Todd and Johnson[6] analyzed the shape of hysteresis friction curves, and these curves were found to be in agreement with hysteresis loops generated using Dahl's equation. Lovell et al.[7–10] verified this hysteresis curves by three-ball experimental testing apparatus at a constant rate and sinusoidal oscillating rate, respectively. In the Lovell's study, the experimental testing apparatus was designed to incorporate three balls, rather than a full bearing (without considering the cage) so as to eliminate the additional friction elements and the hysteresis behavior could be readily determined. In the Lovell's experiments, the balls' diameters (12.7 mm) were bigger and the loads (81.6, 133.5, 185.4 N/ball) were larger. All of the above studies proved that the elastic hysteresis in relatively large ball bearings is an important source under high loads and ultra-low speed conditions. Whether the friction moment caused by elastic hysteresis under lower loads in mini-ball bearing occupies a large proportion in the total bearing's friction moment needs to be studied. In addition, the sources of friction in ball bearings are manifold[11] and other friction sources also need to be known, since the friction moment is an important factor for controlling space instruments. Some experiments[12,13] for the gyroscope bearings proved that the friction moment caused by cage was high and might not be neglected at the onset of bearing. In order to know the friction moment caused by that, a study of the ribbon cage dynamics at ultra-low speeds and its influence on the bearing's total friction moment is carried out in this paper.

More advanced analyses about dynamic behavior of cage, such as the references of Gupta,[14] Meeks,[15,16] and Houpert[17–19] have been developed at higher speeds. Because of the influences of the cage centrifugal force, the skidding phenomenon and the viscous drag of the lubricant between ball and cage, the cage analysis model at higher speed is much more complicated than that at lower speed. The difficulty in their high speed dynamic models is a considerable number of computations in a short final output time, for example, the final output time shown in Ref.[16] was 0.01 s and 2.5 s in Ref.[19]. In spite of the force model at ultra-low speeds can be relatively simply designed, the time step is much smaller than that at higher speed. The time for output results needs to be 3–5 s at least under constant rate and even longer under oscillatory motion. It needs to change the time steps to perform the numerical integration instead of the constant time step in the model. However, changing the time steps makes the program more easily divergent especially under oscillatory motion. How to make sure that the program carries out smoothly and how to improve the final output time are introduced in this paper.

2. Total friction moment of bearing

The total friction moment includes five principal sources[11] of friction in space gyroscope ball bearings. They are the friction moment due to the elastic hysteresis in rolling M_E, the friction moment due to the geometry of the contacting surfaces M_D, the friction moment due to the pivoting on contact ellipse M_S, the friction moment due to the viscous drag of lubricant

M_L, and the friction moment due to the sliding between the cage and balls M_C. M_E, M_D, M_S M_L have to be deduced maturely by static analysis and M_C needs to be analyzed with more complicated dynamic models. According to the analyses by Houpert,[20] the total friction moment M acting on the outer race of bearing is

$$M = \sum^{z}(\mathrm{d}M_L + \mathrm{d}M_E + \mathrm{d}M_D + \mathrm{d}M_S + \mathrm{d}M_C)$$
$$= M_L + \sum^{z}\left(\begin{array}{c}\dfrac{\mathrm{d}M_{Eo}R_i + \mathrm{d}M_{Ei}R_o}{D_w} + \dfrac{\mathrm{d}M_{Do}R_i + \mathrm{d}M_{Di}R_o}{D_w} \\ + \dfrac{\mathrm{d}M_{Si} + \mathrm{d}M_{So}}{2}\sin\beta + \dfrac{(F_\mu^p \pm F_{pbz}^p)R_o}{2}\end{array}\right) \quad (1)$$

where z is the number of balls, D_w is the ball diameter, β is the contact angle, and $\mathrm{d}M_L$, $\mathrm{d}M_E$, $\mathrm{d}M_D$, $\mathrm{d}M_S$, and $\mathrm{d}M_C$ are the individual one ball contribution to the friction moment of lubricant, elastic hysteresis, the geometry of the contacting surfaces, pivoting effects and ball-cage contact, respectively. R_i, R_o are the radii to initial contact point between the ball and inner and outer race, respectively. The formulas of M_L, $\mathrm{d}M_{Ei}$, $\mathrm{d}M_{Eo}$, $\mathrm{d}M_{Di}$, $\mathrm{d}M_{Do}$, $\mathrm{d}M_{Si}$, $\mathrm{d}M_{So}$ and their references are deduced by following Eq. (2). The subscripts i, o represents the inner and outer race, respectively.

$$\begin{cases} M_L = 160 \times 10^{-7}fd_m^3 \\ \mathrm{d}M_E = \frac{3}{16}Q_n(i)b\alpha_r \\ \mathrm{d}M_D = \dfrac{\mu_b Q_n(i)a^2}{R_a}\left(\dfrac{1}{10} + \dfrac{X_2^3 - X_1^3}{4} + \dfrac{3X_1^5 - 3X_2^5}{20}\right) \\ \mathrm{d}M_S = \dfrac{3\mu_b Q_n(i)a}{8}\left[2(X_2^2 - X_1^2) + X_1^4 - X_2^4\right] \end{cases} \quad (2)$$

In Eq. (2), f is a factor depending upon type of bearing and method of lubrication. d_m is the bearing's pitch diameter. $Q_n(i)$ is the normal force between the ith ball and race. The losing energy caused by the hysteresis is thought to be the energy caused by the friction, and the losing energy due to the elastic hysteresis is a small proportion α_r (for metal, usually $0.7\% \leqslant \alpha_r \leqslant 1.0\%$, here $\alpha_r = 0.8\%$). a and b are semimajor and semiminor axes of the contact ellipse respectively. R_a is the Hertz contact radius. $X_1 = x_1/a$, $X_2 = x_2/a$ $(x_2 > 0)$, where x_1, x_2 is the locations of two pure rolling lines respectively on the contact ellipse in Ref.[20] F_{pbz}^p in Eq. (1) is the z_p component in Frame p (introduced later) of the normal ball-cage contact force and $F_\mu^p = \mu F_{pbz}^p$, of which μ is the friction coefficient between the ball and cage and F_{pbz}^p is positive or negative depending upon whether the ball is driving the cage

Table 1 Structure parameters.

Structure parameter	Value
Inner diameter of inner race, d (mm)	4.00
Outer diameter of outer race, D (mm)	9.00
Ball diameter, D_w (mm)	1.30
Number of balls, z	8.00
Contact angular, β (°)	0.00
Inner race conformity, f_i	0.55
Outer race conformity, f_o	0.55
Depth of ribbon cage pocket, k (mm)	0.67
Diameter of cage pocket, d_p (mm)	1.40
Thickness of cage, s (mm)	0.15
Clearance between cage pocket and ball, Λ (mm)	0.02

or vice versa. The calculations of them need to build the cage dynamics so as to obtain M_C. μ_b in Eq. (2) is the friction coefficient between the ball and inner/outer race. In the paper $\mu_b = 0.08$, which is based on the experimental results of four-ball friction machine by professor Tao Dehua in Shanghai University. This value is also consistent with the test results by Houpert with the same oil viscosity (15 CST) in Table 2 in Ref.[21] The oil viscosity in our experiment is 14.8 CST.

3. Cage dynamics analysis

3.1. Coordinate systems

Fig. 1 shows the fixed inertial reference frame $o_I x_I y_I z_I$ (Frame I) with the y_I axis located at the initial position of No. 1 ball. The inner and outer races rotate about the x_I axis with angular velocities w_i, w_o, respectively. The coordinate system $o_c x_c y_c z_c$ (Frame c) is fixed to the cage with the cage geometrical center o_c as its origin. The local coordinate system $o_p x_p y_p z_p$ (Frame p) is fixed to the ith pocket, with the pocket center o_p as its origin. Counterclockwise rotation is designated to be positive, and balls are also numbered counterclockwise. The superscripts I, c and p represent the corresponding reference frame. The ball-cage coordinate system $o_m x_m y_m z_m$ (Frame m), not shown in Fig. 1, rotates about the x_m axis with the theoretical angular velocity w_{bc},

$$\begin{cases} w_{bc} = \dfrac{1}{2}\left[w_i(1-\gamma) + w_o(1+\gamma)\right] \\ \gamma = \dfrac{D_w \cos\beta}{d_m} \end{cases} \tag{3}$$

Let ψ_i be the angular position of the ith ball, the position vector of ith ball center in Frame I is

$$\mathbf{r}_{ob}^I = \begin{bmatrix} 0 \\ \dfrac{d_m}{2}\cos(\psi_i + w_{bc}t) \\ \dfrac{d_m}{2}\sin(\psi_i + w_{bc}t) \end{bmatrix} \tag{4}$$

Let $\boldsymbol{\theta} = [\theta_x, \theta_y, \theta_z]^T$ be the sequential angles obtained by rotating the x, y, z axes from Frame I to Frame c, respectively. The transform matrix $\mathbf{A}_{Ic}$ from Frame I to Frame c is

Fig. 1   Relationship of reference frames.

Let $\mathbf{w}_{oc}^c$ be the cage's angular velocity in Frame c, then

$$\begin{cases} \mathbf{w}_{oc}^c = \boldsymbol{\varphi}[\dot{\theta}_x, \dot{\theta}_y, \dot{\theta}_z]^T \\ \boldsymbol{\varphi} = \begin{bmatrix} \cos\theta_y \cos\theta_z & \sin\theta_z & 0 \\ -\cos\theta_y \sin\theta_z & \cos\theta_z & 0 \\ \sin\theta_y & 0 & 1 \end{bmatrix} \end{cases} \tag{6}$$

In the paper, the superscripts in variables represent the corresponding frame. Let $\mathbf{R}_{oc}^c$ be the offset vector from o_c to o_I in Frame c, then in Frame I, $\mathbf{R}_{oc}^I = \mathbf{A}_{Ic}^{-1}\mathbf{R}_{oc}^c$. As shown in Fig. 2, because the same vector has different value in different frame, the superscripts in the figure were not shown. $\mathbf{r}_{cb}$ is the vector of o_b relative to the o_c, $\mathbf{r}_{cp}$ is the vector of o_p relative to the o_c.

3.2. Ball and ribbon cage contact

The cage type is ball riding design, so only the contact between the ball and cage occurs. Fig. 3 provides three views of the contact status of a ball in its pocket. k is the pocket depth and D_p is the diameter of cage pocket, where $k < D_p/2$. The clearance between the cage pocket and ball is defined as Λ, and $\Lambda = k - D_w/2$. o_p' denotes the pocket curvature center. When the ball center moves along the x_p axis, one point contact may occur. While as the ball center moves along the z_p axis, two contact

$$\mathbf{A}_{Ic} = \begin{bmatrix} \cos\theta_y \cos\theta_z & \cos\theta_x \sin\theta_z + \sin\theta_x \sin\theta_y \cos\theta_z & \sin\theta_x \sin\theta_z - \cos\theta_x \sin\theta_y \cos\theta_z \\ \cos\theta_y \sin\theta_z & \cos\theta_x \cos\theta_z - \sin\theta_x \sin\theta_y \sin\theta_z & \sin\theta_x \cos\theta_z + \cos\theta_x \sin\theta_y \sin\theta_z \\ \sin\theta_y & -\sin\theta_x \cos\theta_y & \cos\theta_x \cos\theta_y \end{bmatrix} \tag{5}$$

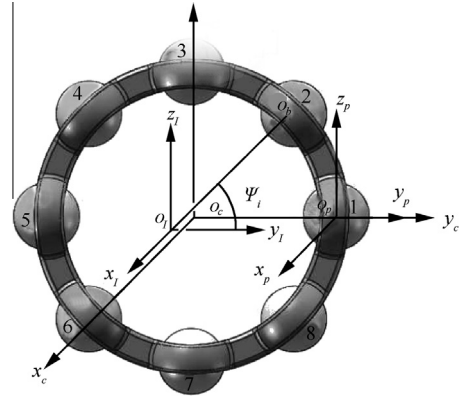**Table 2**   Comparison of maximum total friction moment under two conditions.

Load (N)	$n_o = 2$ r/min			$n_o = 5$ r/min		
	SFMC (μN·m)	SFMO (μN·m)	Increased percentage	SFMC (μN·m)	SFMO (μN·m)	Increased percentage
1	5.34	6.74	26.22	10.06	14.51	44.23
2	8.24	9.73	18.08	13.73	17.01	23.89
3	12.64	14.69	16.22	17.72	21.45	21.05
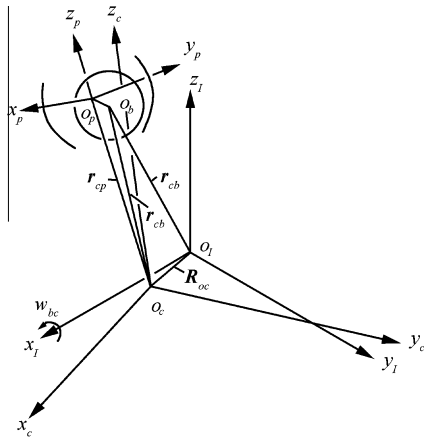
Fig. 2 Locating ball center in frames.
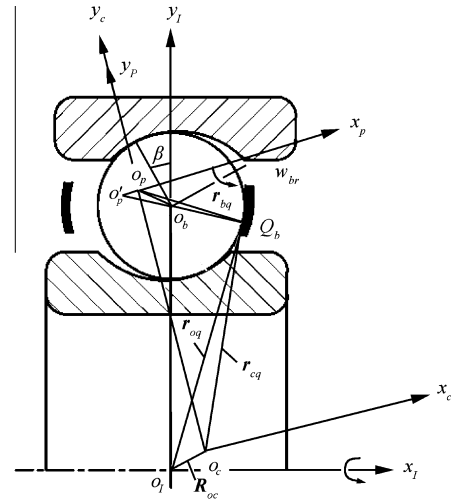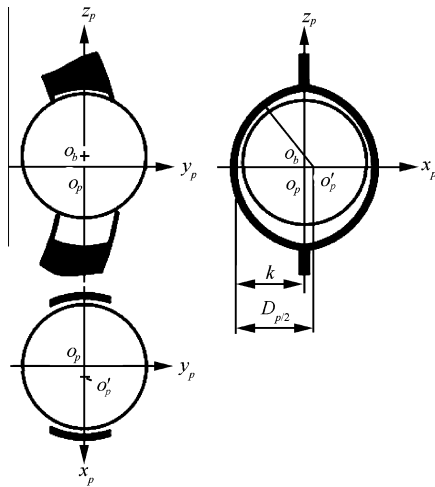

Fig. 3 One ball in its pocket.

points may occur. The contact status can be determined by the position vector of ith ball in Frame p.

The balls and the cage need not always contact. Let the position vector of ball center in Frame p be $\boldsymbol{r}_{pb}^p = [\Delta x, \Delta y, \Delta z]^{\mathrm{T}}$, then three contact cases are considered: one point contact, $\varepsilon \geqslant \nabla, \Delta x \neq 0$, two points contact, $\varepsilon \geqslant \nabla, \Delta x = 0$, no contact, $\varepsilon < \nabla$. And,

$$
\begin{cases}
\varepsilon = \sqrt{\left(|\Delta x| + \left|\frac{D_p}{2} - k\right|\right)^2 + \Delta y^2 + \Delta z^2} \\
\nabla = \frac{D_p}{2} - \frac{D_w}{2}
\end{cases}
$$

As shown in Fig. 4, the ball linear velocity at the contact point Q_b in Frame p is

$$
\boldsymbol{v}_b^p = \boldsymbol{B}_i \boldsymbol{A}_{Ic}(\boldsymbol{w}_{bc}^I \times \boldsymbol{r}_{oq}^I) + \boldsymbol{w}_b^p \times \boldsymbol{r}_{bq}^p \tag{7}
$$

where $\boldsymbol{B}_i = \begin{bmatrix} 1 & 0 & 0 \\ 0 & \cos\psi_i & \sin\psi_i \\ 0 & -\sin\psi_i & \cos\psi_i \end{bmatrix}$ is the transform matrix

from Frame c to Frame p, $\boldsymbol{w}_b^p = [w_{br}\cos\beta, 0, w_{br}\sin\beta]^{\mathrm{T}}$ and $\boldsymbol{w}_{bc}^I = [w_{bc}, 0, 0]^{\mathrm{T}}$, w_{br} is the ball spinning velocity, and $\boldsymbol{r}_{bq}^p$ and $\boldsymbol{r}_{oq}^I$ are the contact vectors from the ball center o_b and o_I to

Fig. 4 Contact between the ball and cage.

Q_b, respectively. $\boldsymbol{r}_{cq}^p$ is the contact vector from the point o_c to Q_b. Let the cage angular velocity vector in Frame c be $\boldsymbol{w}_{oc}^c$, then the cage linear velocity at this contact point in Frame p is

$$
\boldsymbol{v}_c^p = \boldsymbol{B}_i \dot{\boldsymbol{R}}_{oc}^c + (\boldsymbol{B}_i \boldsymbol{w}_{oc}^c) \times \boldsymbol{r}_{cq}^p \tag{8}
$$

The velocity of the ball relative to the cage in Frame p is

$$
\Delta \boldsymbol{v}_{cb}^p = \boldsymbol{v}_c^p - \boldsymbol{v}_b^p \tag{9}
$$

Hertz contact is assumed between the ball and cage here, which is similar to the contact between the balls and inner/outer races.[11] If the contact deformation is $\Delta \delta_{pb}$, the normal contact force between the ball and cage is

$$
\begin{cases}
F_{pbN}^p = K_{pb} \Delta \delta_{pb}^{3/2} \\
\Delta \delta_{pb} = \varepsilon - \nabla
\end{cases} \tag{10}
$$

where K_{pb} is the contact force–deformation coefficient between the ball and cage. For the bearings working under ultra-low oscillatory motion, the lubrication between the ball and cage is boundary lubrication. The contact condition between them is more close to the contact with "dry" film lubrication, so the deduction of K_{pb} is also similar to the ball and race contact force–deformation coefficient[11] with "dry" film lubrication. Once F_{pbN}^p and $\boldsymbol{r}_{pb}^p$ are obtained, the normal contact force vector F_{pbN}^p and its unit vector $\boldsymbol{N}_{pb}^p$ can be known. The tangent relative velocity of ball and cage in Frame p is

$$
\Delta \boldsymbol{v}_{cbT}^p = \Delta \boldsymbol{v}_{cb}^p - (\Delta \boldsymbol{v}_{cb}^p \cdot \boldsymbol{N}_{pb}^p) \boldsymbol{N}_{pb}^p \tag{11}
$$

Let the tangential contact force vector be F_{pbT}^p, and the deduction of it is

$$
F_{pbT}^p = -\mu F_{pbN}^p \frac{\Delta \boldsymbol{v}_{cbT}^p}{|\Delta \boldsymbol{v}_{cbT}^p|} \tag{12}
$$

where μ is the friction coefficient between ball and cage, which will be introduced in experiments. Oil damping force is not taken into account because the speed is ultra-low. Considering the gravity of cage $\boldsymbol{G}_c$ and summing up all the ball-cage contact forces and moments, the resultant force and moment vector on the cage in Frame c are

$$\begin{cases} \boldsymbol{F}^c = \sum_{i=1}^{z} \boldsymbol{B}_i^{-1}\left(F_{pbN}^p + F_{pbT}^p\right) + \boldsymbol{G}_c \\ \boldsymbol{M}^c = \sum_{i=1}^{z} \boldsymbol{B}_i^{-1}\left[\boldsymbol{r}_{cq}^p \times \left(F_{pbN}^p + F_{pbT}^p\right)\right] \end{cases} \tag{13}$$

3.3. Cage dynamic equations of motion

The basic motion equations of cage are:

$$\boldsymbol{v}_{oc}^c = \dot{\boldsymbol{R}}_{oc}^c = [v_{xoc}^c, v_{yoc}^c, v_{zoc}^c]^{\mathrm{T}} \tag{14}$$

$$\begin{bmatrix} \dot{\theta}_x \\ \dot{\theta}_y \\ \dot{\theta}_z \end{bmatrix} = \begin{bmatrix} \cos\theta_z/\cos\theta_y & -\sin\theta_z/\cos\theta_y & 0 \\ \sin\theta_z & \cos\theta_z & 0 \\ -\tan\theta_y\cos\theta_z & \tan\theta_y\sin\theta_z & 1 \end{bmatrix} \begin{bmatrix} w_{xoc}^c \\ w_{yoc}^c \\ w_{zoc}^c \end{bmatrix} \tag{15}$$

where $\boldsymbol{w}_{oc}^c = \begin{bmatrix} w_{xoc}^c, & w_{yoc}^c, & w_{zoc}^c \end{bmatrix}^{\mathrm{T}}$. Since the cage structure is symmetrical, there are no products of inertia, and the moments of inertia about the x_c axis, y_c axis, and z_c axis are J_x, J_y, J_z, respectively. Once the total force vector $\boldsymbol{F}^c = [F_x^c, F_y^c, F_z^c]^{\mathrm{T}}$ and total moment vector $\boldsymbol{M}^c = [M_x^c, M_y^c, M_z^c]^{\mathrm{T}}$ in Frame c are calculated, based on the Euler law, the accelerations can be calculated as follows:

$$\begin{cases} \dfrac{F_x^c}{m_c} = \dfrac{\mathrm{d}V_{xoc}^c}{\mathrm{d}t} + w_{yoc}^c V_{zoc}^c - w_{zoc}^c V_{yoc}^c \\[2mm] \dfrac{F_y^c}{m_c} = \dfrac{\mathrm{d}V_{yoc}^c}{\mathrm{d}t} + w_{zoc}^c V_{xoc}^c - w_{xoc}^c V_{zoc}^c \\[2mm] \dfrac{F_z^c}{m_c} = \dfrac{\mathrm{d}V_{zoc}^c}{\mathrm{d}t} + w_{xoc}^c V_{yoc}^c - w_{yoc}^c V_{xoc}^c \\[2mm] M_x^c = J_x\dfrac{\mathrm{d}w_{xoc}^c}{\mathrm{d}t} + (J_z - J_y)w_{yoc}^c w_{zoc}^c \\[2mm] M_y^c = J_y\dfrac{\mathrm{d}w_{yoc}^c}{\mathrm{d}t} + (J_y - J_z)w_{xoc}^c w_{zoc}^c \\[2mm] M_z^c = J_z\dfrac{\mathrm{d}w_{zoc}^c}{\mathrm{d}t} + (J_y - J_x)w_{xoc}^c w_{yoc}^c \end{cases} \tag{16}$$

Eqs. (14)–(16) form a complete set of dynamic equations for the ribbon cage. The conventional fourth-order Runge–Kutta method[15] is used to perform the numerical integration, and the vectors $\boldsymbol{R}_{oc}^c = [R_{xoc}^c, R_{yoc}^c, R_{zoc}^c]^{\mathrm{T}}$, $\boldsymbol{\theta} = [\theta_x, \theta_y, \theta_z]^{\mathrm{T}}$, $\boldsymbol{v}_{oc}^c = [v_{xoc}^c, v_{yoc}^c, v_{zoc}^c]^{\mathrm{T}}$, $\boldsymbol{w}_{oc}^c = [w_{xoc}^c, w_{yoc}^c, w_{zoc}^c]^{\mathrm{T}}$ can be determined.

3.4. Balls motion

In order to simplify the model, each ball's motion considers only two degree-of-freedom. Each ball orbits the bearing axis (w_{bc}), and revolves about its own axis (w_{br}) simultaneously. Referring to the Fig. 5, at the start or when oscillation occurs, the ball's motion is thought to be driven by motor and the start or oscillatory acceleration ε is supposed to be constant. The ball's motion is
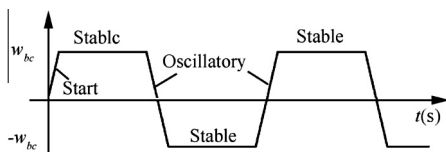
Fig. 5 Motion model of ball under oscillatory motion.

$$\begin{cases} w_{bc} = \dfrac{1}{2}(1+\gamma)\varepsilon t(i) \\[2mm] w_{br} = \dfrac{d_m}{2D_w}(1-\gamma)(1+\gamma)\varepsilon t(i) \end{cases} \tag{17}$$

Once the orbital speed of ball w_{bc} runs up to the setting value, the ball motion is thought to be stable and $\varepsilon = 0$. At the stable stage, if some ball is in contact with the cage, the ball/cage contact force then affects its orbital and revolutionary speed. The motion of ball is affected by ball/cage contact force F_{pbN}^p. Three different conditions are considered as follows:

Condition 1: If the ith ball runs at the unload area, there is a small clearance between the ball and race. A pure rolling occurs.

$$\begin{cases} \left(I_b + m_b\left(\dfrac{d_m}{2}\right)^2\right)\dot{w}_{bc} = \pm F_{pbz}^p\dfrac{d_m}{2} - F_\mu^p\dfrac{D_w}{2} \\[2mm] \dot{w}_{br} = \dfrac{d_i}{D_w}\dot{w}_{bc}\,(\text{if } w_i = 0) \end{cases} \tag{18}$$

where I_b is the ball inertia about its center axis, m_b is the ball mass and d_i is the diameter of contact point between the ball and inner race. Because only two degree-of-freedom of the ball is considered, F_{pbz}^p is z_p component of F_{pbN}^p in z axis direction in Frame p.

Condition 2: If the ith ball runs at the load area and $F_{pbN} \leqslant \mu Q_n(i)$, no slipping occurs and w_{bc} and w_{br} are unchangeable.
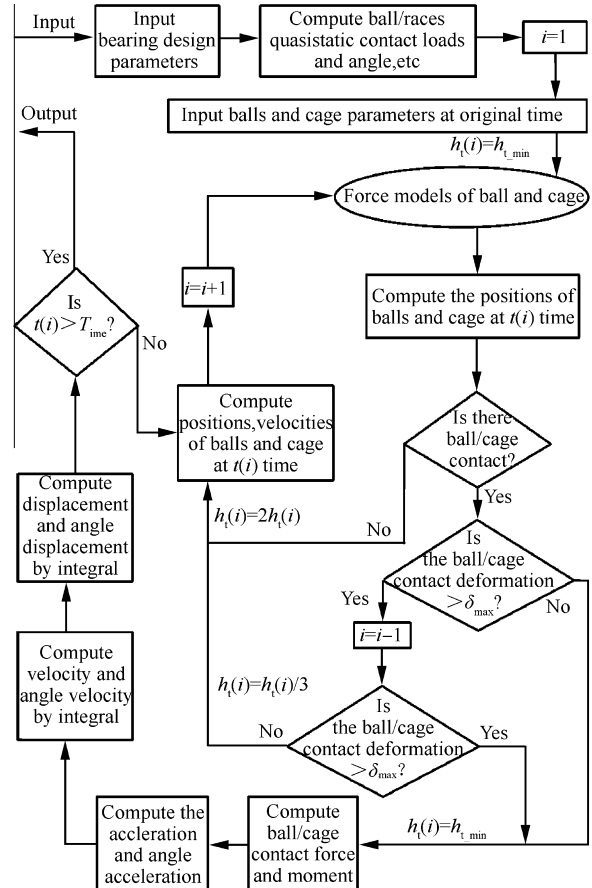
Fig. 6 Program frame of cage dynamic analysis.

Condition 3: If the ith ball runs at the load area and $F_{pbN} > \mu Q_n(i)$, a small slipping occurs. According to the model of Meeks,[15] the slipping forces between the ball and inner/outer races are

$$\begin{cases} F_{si} = \mu Q_n(i)\dot{s}_i/\dot{s}_{roll} \\ F_{so} = \mu Q_n(i)\dot{s}_o/\dot{s}_{roll} \end{cases} \tag{19}$$

where $\dot{s}_i$ and $\dot{s}_o$ are the slipping velocities of the inner and outer race, and $\dot{s}_{roll}$ is the rolling velocity of ball. So according to the force along the orbit path and moment about ball center in Frame p,

$$\begin{cases} \pm F_{pbN} - F_{si} - F_{so} = m_b \ddot{s}_b \\ (F_{so} - F_{si} - F_{pbT})\dfrac{D_w}{2} = I_b \dot{w}_{br} \end{cases} \tag{20}$$

$\dot{s}_b$ is the slipping velocity of ball. The relationship about them is

$$\begin{cases} \dot{s}_i + \dot{s}_o = 2\dot{s}_b \\ \dot{s}_o - \dot{s}_i = \dfrac{D_w w_{br}}{2} \end{cases} \tag{21}$$

3.5. Integration procedures with variable time steps

Because the bearing's speed and the deformation between the cage and balls are small, the time step also needs to be small, which makes the computational program time-consuming. So, variable time steps are used in the program. However, the variable time steps make the program divergent easily.

In order to make sure that the program is carried out smoothly, the maximum deformation δ_{max} and minimum deformation δ_{min} are introduced. δ_{max} in the paper is supposed to be the maximum deformation between the ball and race based on the quasi-static analyses and $\delta_{min} = \delta_{max}/100000$. When contact occurs at the beginning, which is controlled by δ_{min}, the time step is then chosen to be the smallest, and $h_t(i) = h_{t\_min}$ (about 1×10^{-8} s–3×10^{-8} s). If $\Delta\delta_{pb} \leqslant 0$, large time steps are continued to be amplified, and $h_t(i) = 2h_t(i)$. If $\Delta\delta_{pb} > \delta_{max}$, the time steps must be reduced, and $h_t(i) = h_t(i)/3$. The program frame is shown as Fig. 6.
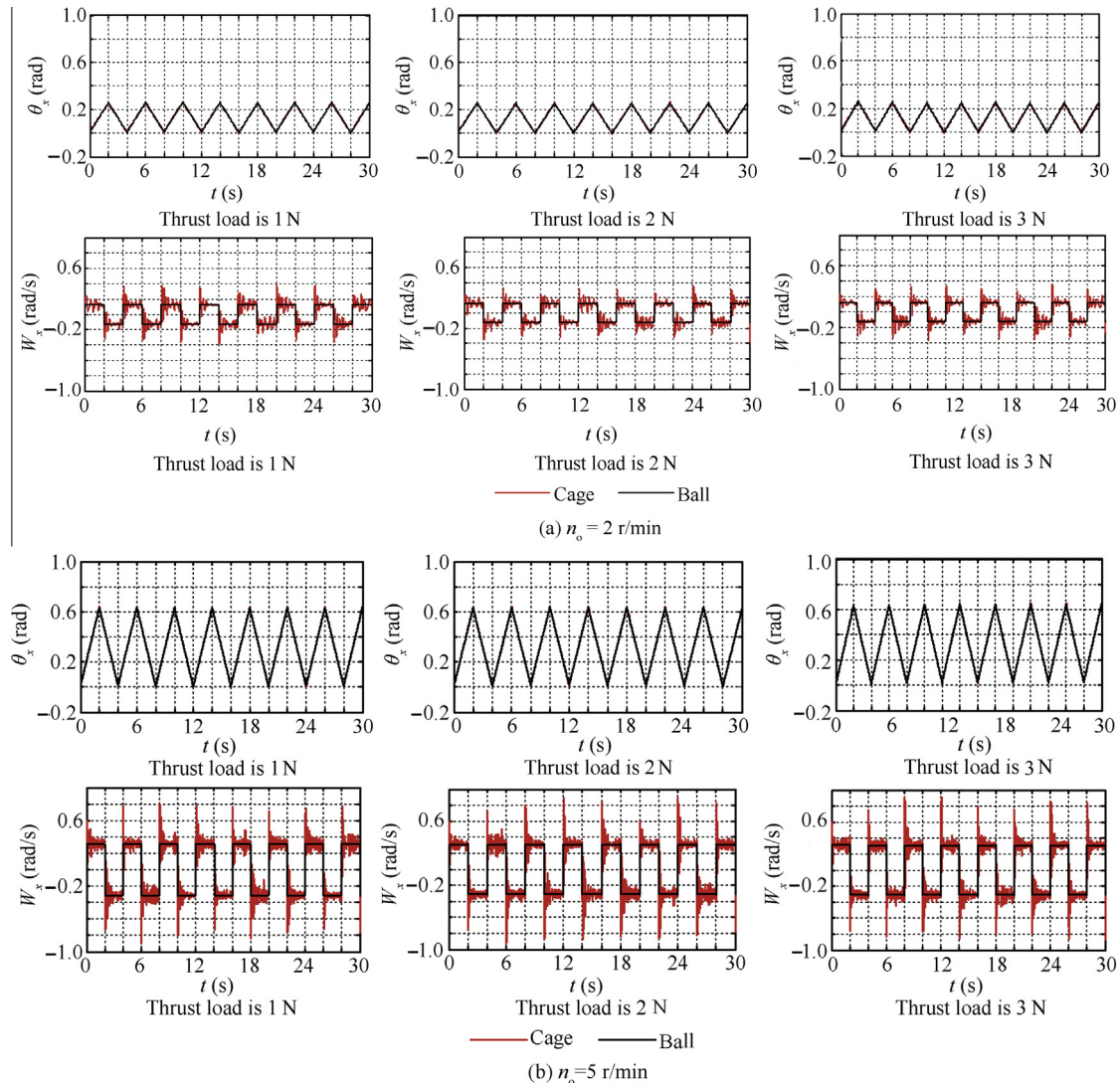
Fig. 7   Cage angular displacement and angular velocity about x_I axis.

4. Calculated results

One size of mini-ball gyroscope bearing is used. Its structure parameters are given in Table 1.

According to the working conditions of gyroscope bearings, the outer race rotational speeds n_o of bearing are ± 2 r/min and ± 5 r/min. The thrust loads are 1 N, 2 N, 3 N. Fig. 7(a) and (b) show the program results of orbital angular and angular velocity of No. 1 ball (black line) and cage (red line) about the bearing rotational axis under oscillatory motion. From the results, the cage's angular velocity fluctuates around the ball's angular velocity. The motion of the ball immediately reacts with the motion of outer race, and the angular velocities of the cage vary more than those of the ball. This phenomenon means that the ball-cage contact force has an obvious influence on the cage motion than on the ball motion. At the same speed, there is no obvious change of cage motion with increasing thrust load. When oscillation occurs, the cage motion fluctuates more obviously than that at a constant rate, especially at ± 5 r/min.

Fig. 8 shows the program results of M_C. The normal force between the ball and cage can be positive or negative, so the value of M_C might be positive or negative. When $n_o > 0$, the positive value of M_C denotes that the contact force drives the cage's rotation, the negative value of M_C denotes that the contact force retards the cage's rotation, and zero means that there is no friction force. When $n_o < 0$, it is contrary to the positive or negative value of M_C. From the results, the thrust load has little influence on M_C at the same speed and M_C increases clearly with the increasing input speed. Through analyses, only the contact force that drives the cage's rotation will make M increase, so the corresponding M_C is reserved for further analyses. Obviously M_C at ± 5 r/min are larger than M_C at ± 2 r/min.

Fig. 9 shows the friction moments caused by five sources M_E, M_D, M_S, M_L, M_C and the bearing's total friction moment M (blue line). From the results, when oscillation occurs, M_C is obviously larger than other friction moments, especially at ± 5 r/min. So the proportion of M_C in M occupies the main part (from the results, about $> 50\%$) at the onset of every
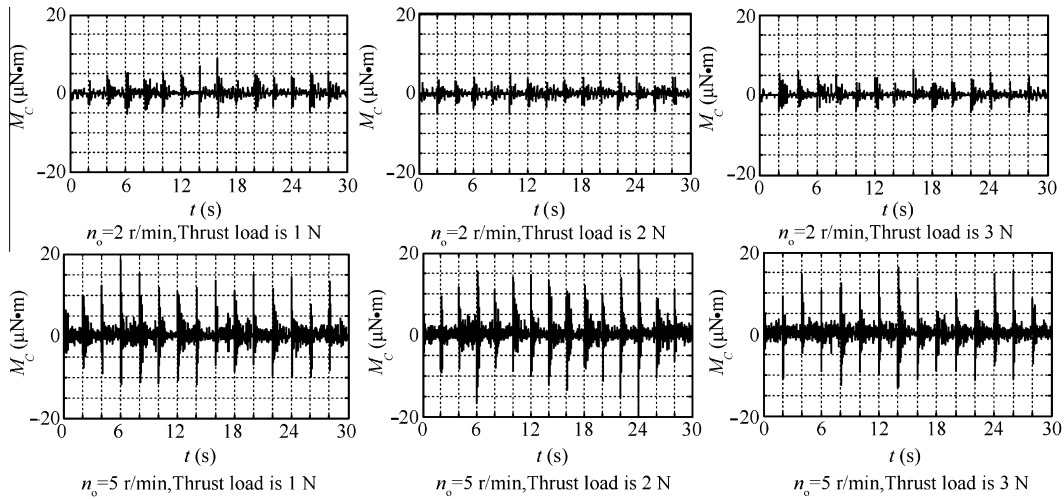

Fig. 8 M_C versus time under oscillatory motion.

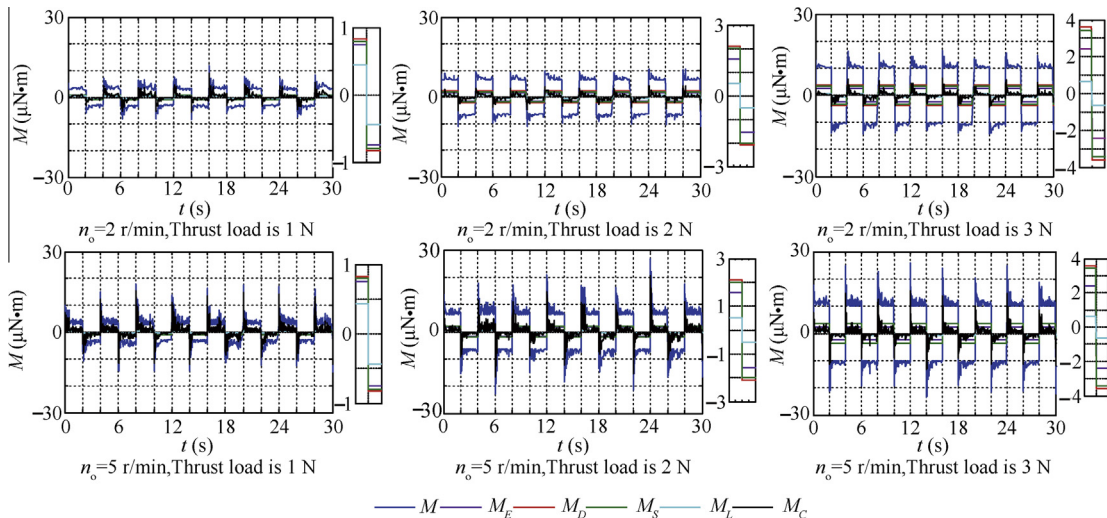$$— M \quad — M_E \quad — M_D \quad — M_S \quad — M_L \quad — M_C$$

Fig. 9 M, M_E, M_D, M_S, M_L and M_C versus time under oscillatory motion.

oscillation. When the bearing runs after a short time (about 1 s) of every oscillation, M_C rapidly reduces to a small value (nearly to zero at ± 2 r/min), so the proportion of M_C in M turns to be smaller and the proportions of M_E, M_D, M_S occupy the mainly part in M. Referring to Eq. (2), M_E, M_D and M_S increase with the increasing thrust load and M_C is almost unchanged with the increasing thrust load, so the proportion of M_C decreases with the increasing load. The maximum M when the bearing starts to run from rest is defined as the starting friction moment of bearing at a constant rate (SFMC). Extracting the maximum M of each 2 s oscillation period and then averaging these maximum data by program, the mean friction moment is defined as the starting friction moment of bearing under oscillatory motion (SFMO).

From Table 2, SFMO is obviously larger than SFMC and the increased percentage is at least more than 15%.

In order to illustrate clearly, Fig. 10(a) shows M with only two different thicknesses of cage ($s = 0.15$ mm and $s = 0.20$ mm) and Fig. 10(b) shows M with four different

thicknesses ($s = 0.15$ mm, $s = 0.20$ mm, $s = 0.25$ mm, and $s = 0.30$ mm) versus time under oscillatory motion. From the results, M increases with the increasing thickness as a whole. When $s = 0.15$ mm or $s = 0.20$ mm, M increases a little, but when $s = 0.25$ mm or $s = 0.30$ mm, M increases clearly. Fig. 11 shows M with different clearance Λ ($\Lambda = 0.01$–0.05 mm) between the cage pocket and ball versus time under oscillatory motion. From the results, M also increases with the increasing clearance as a whole. When the clearance is from 0.01 mm to 0.03 mm, M increases a little, but when $\Lambda = 0.04$ mm or $\Lambda = 0.05$ mm, M increases clearly. This fact is very important for designers when selecting the dimensional tolerance of cage pocket. For both two parameters, M increases clearly at ± 5 r/min than at ± 2 r/min. From the maximum value and range of M, the Λ is very important parameter and the influence of it on M seems much more sensitive. Despite that smaller s and smaller Λ are better to reduce the bearing's friction moment it is worthwhile to note that smaller parameters require more strict processing techniques.
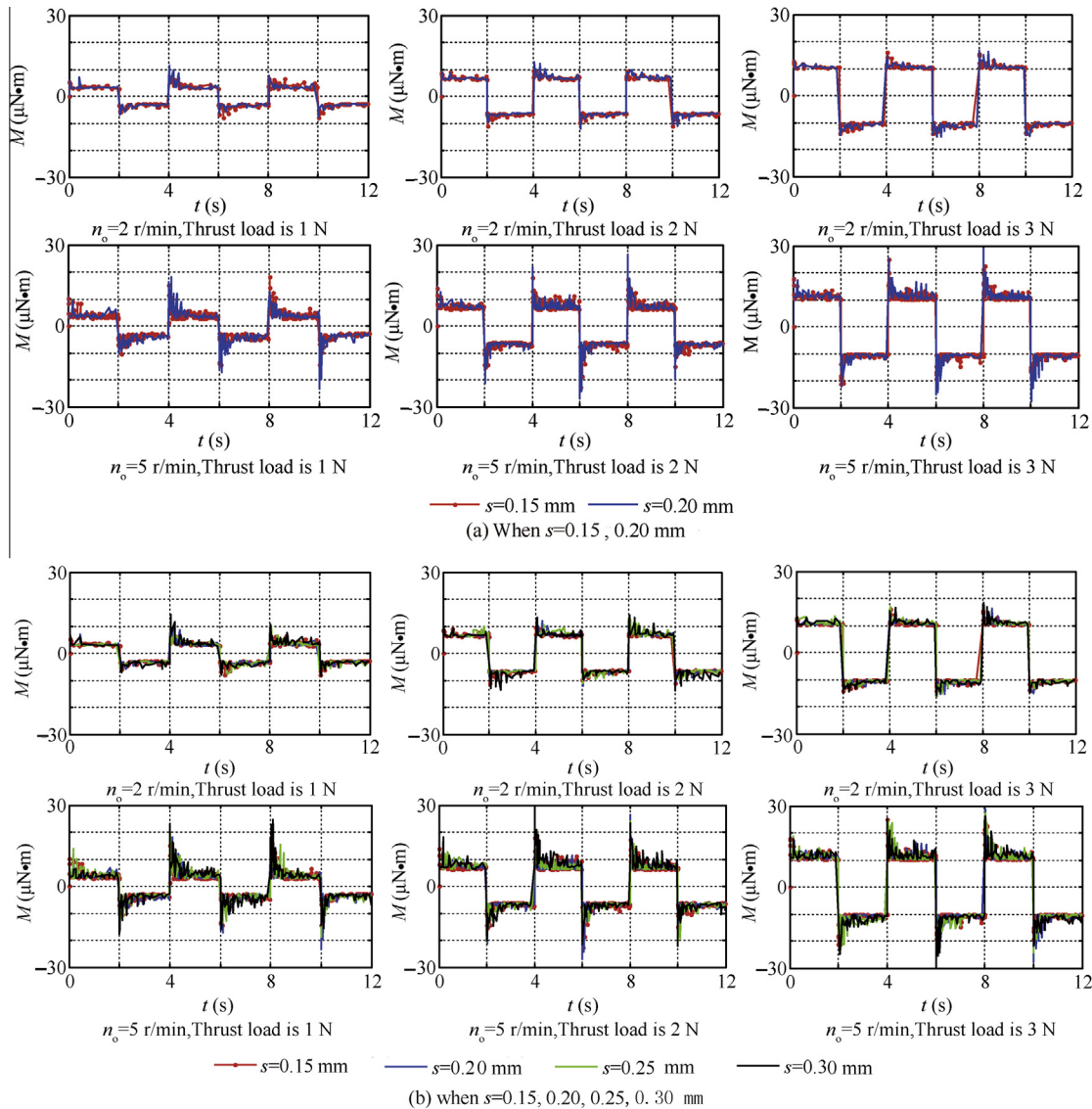

Fig. 10 M with different thicknesses versus time under oscillatory motion.
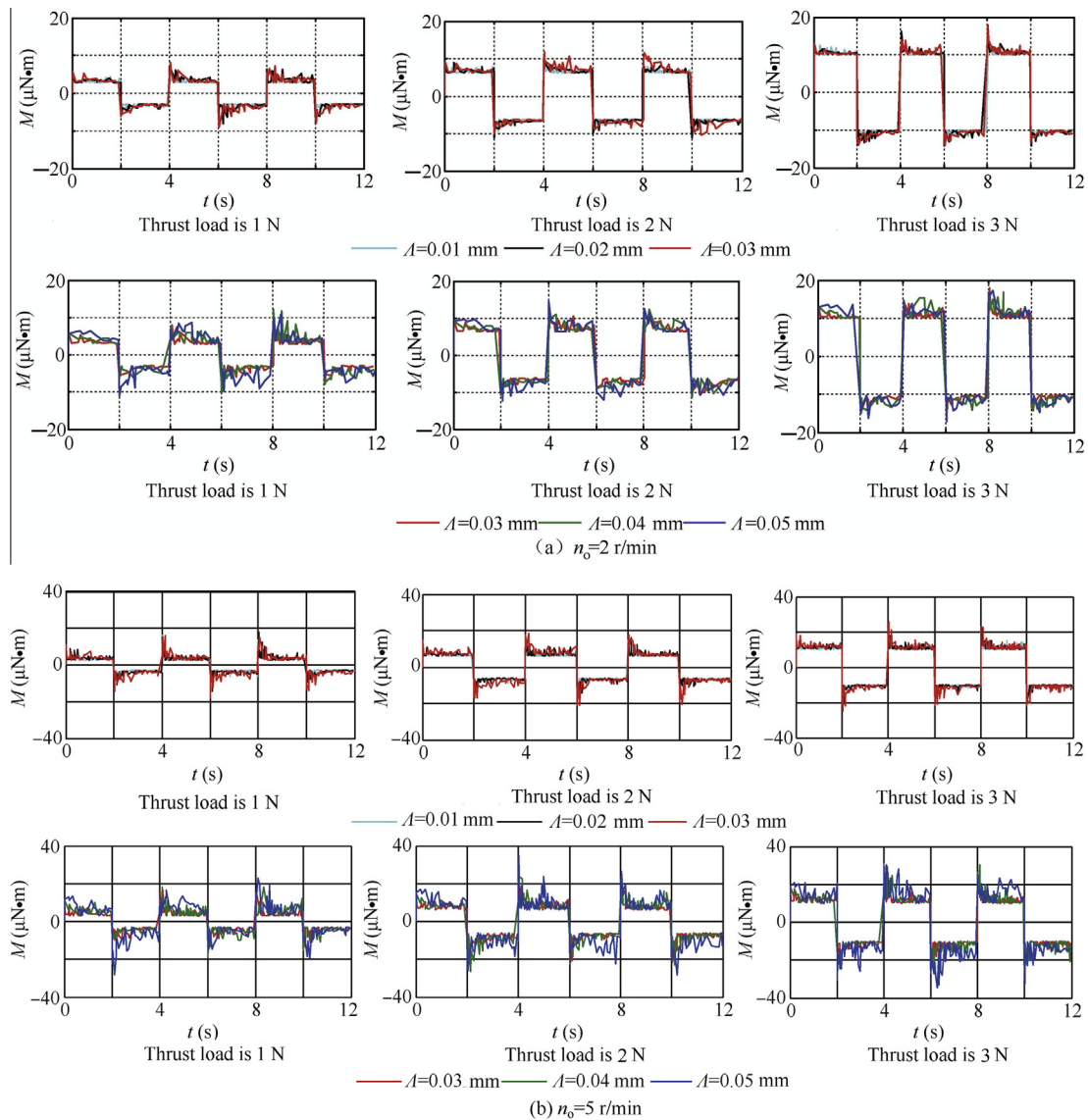
Fig. 11 M with different clearances versus time under oscillatory motion.

Table 3 Comparison of measured results and calculated results at a constant rate.

| Load (N)	Measured results (μN•m)				Calculated results (μN•m)		
	SFMC			RFMC	SFMC		RFMC
	Minimum value	Mean value	Maximum value	Span	2 r/min	5 r/min	Value
1	4.49	8.66	16.38	4–9	5.34	10.06	2.81
2	8.96	17.88	26.98	7–13	8.24	13.73	6.21
3	14.03	23.15	35.92	12–16	12.64	17.72	10.11

5. Measurements

5.1. Measuring friction moment of bearing at a constant rate

At present, the friction moment testers which can be used to measure the starting friction moment at a constant rate (SFMC) and the running friction moment (RFMC, when the bearing runs steadily) at a constant rate are feasible. However,

they cannot work under oscillatory motion. So the calculated SFMC and RFMC were compared with the experimental results respectively at a constant rate.

Table 3 gives the measured results of ten bearings by YZC-II friction moment tester[2] with the same parameters in Table 1. The SFMC of each bearing was measured 15 times forward or backward rotation, respectively. Because the YZC-II tester has no set value about speed parameter when testing SFMC,

(a) Tester

(b) Partial enlarged drawing of
ball and half ribbon cage pocket
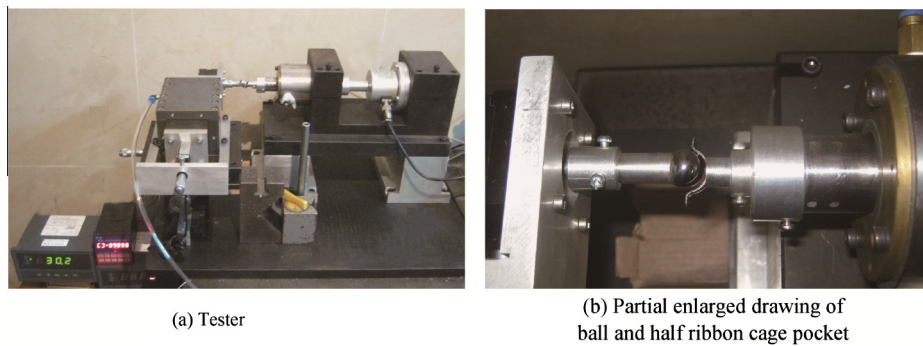
Fig. 12   Tester of measuring the friction coefficient between the ball and cage pocket.

Table 4   Measuring results of friction coefficient between the ball and cage.

Pressure (N)	Speed (r/min)	Lubrication	Friction coefficient	
			Span	Average
5–20	2	A drop of T4 oil	0.05–0.11	0.09
5–20	8	A drop of T4 oil	0.05–0.12	0.08
5–20	8	No oil	0.15–0.20	0.18

according to the operational principle of tester, once the magnitude of the induction moment is equal to the total friction moment of bearing, the bearing will start to run at a ultra-low different speed (about 2–5 r/min). So the measured SFMC results will be compared with the calculated SFMC results at both 2 r/min and 5 r/min.

From the program results, when the bearing runs after a short time, M_C rapidly reduces almost to zero, so only the sum of M_E, M_D, M_S, M_L is thought to be the calculated RFMC. In comparison, the measured results are slightly bigger than the calculated results. That is because except M_E, M_D, M_S, M_L M_C, part of the measured friction moment is produced by structure errors, machining errors, etc. In addition, the friction coefficient for computation is still a crude approximation of the actual conditions, and the differences between the measured results and the computed results are unavoidable. The trends from the calculated SFMC to RFMC are found to be consistent with the measured results with increasing load, so the program at a constant rate is credible.

5.2. Measuring friction coefficient between the ball and cage

Referring to Fig. 12, the friction coefficient between the ball and cage which was used in the model was measured by the following tester to get a more credible value. As shown in Fig. 12(a), the tester includes: torque indictor, pressure indictor, differential head, pressure sensor, three dimensional adjustable table, air-guide, motor, ball and the half pocket of cage, air-bearing, static torque sensor, support of air-bearing and torque sensor, foundation support.

Because the friction between the ball and cage was so small, air bearing was used on the whole supporting system, such as air-guide (number 6) and air-bearing (number 9). The pressure was applied on the ball/cage through pressure sensor (number 4). When the motor drove the ball rolling at lower speed, the friction moments between the ball and pocket versus time were

measured by static torque sensor (number 10). The ball diameter was 12.7 mm in experiment. The friction coefficients were measured under different forces (5–20 N) and two different velocities (2 r/min and 8 r/min). Through data processing, Table 4 shows the results. When there was oil lubrication, the friction coefficients changed about 0.05–0.12, the average of them were 0.09 at 2 r/min and 0.08 at 8 r/min, respectively. When there was no oil lubrication, the friction coefficients changed about 0.15–0.20.

From the measured data, it is difficult to find the relationships between the friction coefficients and velocities or forces under the boundary lubrication conditions, so the changing law of friction coefficients under oscillatory motion cannot be accurately described in the model. Based on the average friction coefficients in Table 4 and considering measuring result through the four-ball friction machine by Professor Tao DH and Ref.[21], the friction coefficients in all contact areas (ball/race and ball/cage contacts) in the model were all roughly taken to be 0.08.

6. Conclusions

(1) The model of calculating the friction moments of mini-bearings under ultra-low oscillatory motion has been built in the paper. The calculated SFMC and RFMC with the model were compared with the measured results at a constant rate at 2 r/min and 5 r/min, respectively. The good trends with different loads between the measured and computational results proved that the computational model at a constant rate was credible. The model under oscillatory motion needs to be further verified by experiments, since the authors are not aware of any existing work in the literature that solves the relevant problems and there are no testers at present to measure friction moments of this kind of precision space gyroscope mini-bearings

under oscillatory motion. However, the changing tendency of calculated results and conclusions under oscillatory motion are given to optimize the cage design.

(2) The ball-cage contact force has an obvious influence on the cage motion than on the ball motion. When oscillation occurs, the cage motion fluctuates more obviously than that at a constant rate, especially at higher speed.

(3) Since the thrust load has no influence on M_C but more influence on other sources of friction moments and the rotational speed has an obvious influence on M_C, the proportion of M_C in M decreases with the increasing load and increases with the increasing input speed. When oscillation occurs, M_C is obviously larger than other friction moments and the proportion of it in M occupies about 50%. When the bearing runs after about 1s of every oscillation, M_C reduces rapidly to a small value and M_E, M_D, M_S occupy the main part in M.

(4) From the program results of bearing example, SFMO is obviously larger than SFMC and the increased percentage is more than 15%. The analyses of different thicknesses of cage and different clearances between cage pocket and ball show that the influence of clearance on M seems much more sensitive and the smaller thickness and clearance are preferred.

Acknowledgments

References

1. Ebert FJ. Fundamentals of design and technology of rolling element bearings. *Chin J Aeronaut* 2010;**23**(1):123–36.
2. Jiang SN, Chen XY, Gu JM, Yu LM, Shen XJ. Analysis of friction torque of sensitive ball bearing under low speed. *Chin Mech Eng* 2010;**21**(05):510–4 [Chinese].
3. Dahl PR. *A solid friction model*. 1968. Report No.: SAMSO-TR-77-131.
4. Dahl PR. *Measurements of solid friction parameters of ball bearings*. 1978. Report No.: TR-0077(2901-03)-3.
5. Todd MJ, Stevens KT. *Friction torque of angular contact ball bearings with different conformities*. 1978. Report No.: ESA-CR(P)-1221.
6. Todd MJ, Johnson KL. A model for Coulomb torque hysteresis in ball bearings. *Int J Mech Sci* 1987;**29**(5):339–54.
7. Lovell MR, Khonsari MM, Marangoni RD. Evaluation of ultra-low-speed jitter in rolling balls. *J Tribol* 1992;**114**(3):589–94.
8. Lovell MR, Khonsari MM, Marangoni RD. Low-speed friction torque on balls undergoing rolling motion. *Tribol Trans* 1993;**36**(2):290–6.
9. Lovell MR, Khonsari MM, Marangoni RD. The response of balls undergoing oscillatory motion: crossing from boundary to mixed lubrication regimes. *J Tribol* 1993;**115**(2):261–6.
10. Lovell MR, Khonsari MM, Marangoni RD. Frictional analysis of MoS2 coated ball bearings-A three-dimensional finite element analysis. *J Tribol* 1997;**119**(4):754–63.
11. Harris TA. *Rolling bearing analysis*. 3rd ed. 2001. p. 193–7, 446–76, 506–8.
12. Li JH, Deng SE, Ma CM. Analysis of friction moment factors of gyroscope frame sensitive bearingsJ. *Bearing* 2006(7);4–7 [Chinese].
13. Xi YJ, Ruan WF, Li H, Fang F, Zhang JJ, Wang P. Development of low friction torque of bearings. *Bearing* 2002(10);13–27 [Chinese].
14. Gupta PK. Dynamics elements in high-speed solid lubricated ball bearing. *Tribol Trans* 1983;**26**(3):393–400.
15. Meeks CR, Ng KO. The dynamics of ball separators in ball bearings – part 1: analysis. *Tribol Trans* 1985;**28**(3):277–87.
16. Meeks CR. The dynamics of ball separators in ball bearings – part 2: results of optimization study. *Tribol Trans* 1985;**28**(3):288–95.
17. Houpert L. CAGEDYN: a contribution to roller bearing dynamic calculations part I: basic tribology concepts. *Tribol Trans* 2010;**53**(3):1–9.
18. Houpert L. CAGEDYN: a contribution to roller bearing dynamic calculations. Part II: description of the numerical tool and its outputs. *Tribol Trans* 2010;**53**(3):10–21.
19. Houpert L. CAGEDYN: a contribution to roller bearing dynamic calculations. Part III: experimental validation. *Tribol Trans* 2010;**53**(3):848–59.
20. Houpert L. Numerical and analytical calculations in ball bearings. *Proceedings of 8th European mechanisms and tribology symposium*. Toulouse, France; 1999. p. 283–90.
21. Houpert L, Leenders P. A study of mixed lubrication in modern deep groove ball bearings. *Proceedings of 11th Leeds-Lyon symposium*. Leeds, England; 1984.

Jiang Shaona is a Ph.D. student in Research Institute of Bearings, Shanghai University. Her main research interests are dynamic analysis of bearing and the analysis of friction mechanism of rolling bearing.

Chen Xiaoyang is a Professor of School of Mechatronical Engineering and Automation of Shanghai University. His research interest includes contact mechanics and profile optimization of roller bearings, tribology or mechanical design and test. He is active in the area of theory and test of EHL, as well as dynamic analysis of ball bearings.

Gu Jiangming is a Professorate senior engineer and manager of Shanghai Tianan Bearing Co., Ltd. His main research interests are product development and analysis of rolling bearing properties.